# Effect of phonon confinement on the thermal conductivity of In$_{0.53}$Ga$_{0.47}$As nanofilms

Jungwon Kim, Hoon Kim, Mehmet Emin Kilic, Chhatrasal Gayner, Rachel Koltun, Hwanjoo Park, Aloysius Soon, John Bowers, Chris Palmstrøm, and Woochul Kim

## Articles you may be interested in

Reduced thermal conductivity of Si/Ge random layer nanowires: A comparative study against superlattice counterparts
Journal of Applied Physics **123**, 244303 (2018); 10.1063/1.5030711

Measuring the thermal properties of anisotropic materials using beam-offset frequency domain thermoreflectance
Journal of Applied Physics **123**, 245110 (2018); 10.1063/1.5033966

Explicit screening full band quantum transport model for semiconductor nanodevices
Journal of Applied Physics **123**, 244501 (2018); 10.1063/1.5031461

Carrier dynamics and optical nonlinearities in a GaN epitaxial thin film under three-photon absorption
Journal of Applied Physics **123**, 243101 (2018); 10.1063/1.5027395

Structural and electronic properties of a-edge dislocations along $\langle 1\text{-}100 \rangle$ in GaN
Journal of Applied Physics **123**, 244301 (2018); 10.1063/1.5034198

Carrier scattering mechanisms limiting mobility in hydrogen-doped indium oxide
Journal of Applied Physics **123**, 245102 (2018); 10.1063/1.5033561

# Effect of phonon confinement on the thermal conductivity of In$_{0.53}$Ga$_{0.47}$As nanofilms

Jungwon Kim,[1,a)] Hoon Kim,[1,a)] Mehmet Emin Kilic,[2] Chhatrasal Gayner,[1] Rachel Koltun,[3] Hwanjoo Park,[1] Aloysius Soon,[2] John Bowers,[3] Chris Palmstrøm,[3] and Woochul Kim[1,b)]

[1]*School of Mechanical Engineering, Yonsei University, Seoul, South Korea*
[2]*Department of Materials Science and Engineering, Yonsei University, Seoul, South Korea*
[3]*Materials Department, University of California, Santa Barbara, California 93106, USA*

Over the past few decades, significant progress has been made to manipulate thermal transport in solids. Most of the effort has focused on reducing the phonon mean free path through boundary scattering. Herein, we demonstrate that the phonon confinement effect can also be used as a tool for managing thermal transport in solids. We measured the thermal conductivities of 10–70-nm-thick In$_{0.53}$Ga$_{0.47}$As nanofilms and found that the thermal conductivities decrease as the film thickness decreases. However, the reasons for this reduction differ for films with different thicknesses. The thermal conductivity of the 30- and 70-nm-thick In$_{0.53}$Ga$_{0.47}$As nanofilms decreases because of severe phonon boundary scattering. Our analysis indicates that phonon confinement occurs in the 10- and 20-nm-thick In$_{0.53}$Ga$_{0.47}$As nanofilms, which modifies phonon dispersion leading to changes in the phonon group velocity and the Debye temperature. These experimental and theoretical results could help to elucidate the phonon confinement effect in nanomaterials as well as establish a platform for understanding nanoscale thermal physics. *Published by AIP Publishing.*
https://doi.org/10.1063/1.5030178

## I. INTRODUCTION

The transistor was invented in 1947 and after 70 years, we are immersed in smart devices such as computers and smartphones. This revolutionary development was possible mainly due to the semiconductor, whose *electrical conductivity* can be tuned over several orders of magnitude.

On the other hand, the methods of manipulating thermal transport in materials remain rudimentary. Thus, over the past few decades, researchers have been focusing on expanding the thermal limits of materials by means of nanostructuring.[1] This is because nanostructuring can affect two length scales in phonon transport: the phonon mean free path (MFP) and wavelength. The effects of these two characteristic length scales on phonon transport can be categorized into three regimes: bulk like, boundary scattering (or Casimir), and confinement.[2] When the size of nanostructures is less than the phonon MFP, the thermal conductivity decreases owing to severe boundary scattering. Ever since the pioneering work of Li *et al.*,[3] this phenomenon has been extensively studied and demonstrated.[3–10]

When the thickness of low-dimensional materials is small/comparable to the dominant phonon wavelength, the spatial confinement from the boundaries could affect the phonon properties, such as the phonon density of states (DOS), group velocity, and heat capacity.[10–14] The thermal conductivity $k$ is a function of specific heat per frequency, $C_v$, phonon group velocity, $v_g$, and MFP, $l$, integrated over a frequency, $\omega$. If the physical size of a crystal is much less than the phonon MFP and smaller than or comparable to the

phonon wavelength, the phonon confinement is important and affects the thermal conductivity due to the modified phonon dispersion relation, which leads to changes in both the speed of sound $c_s$ and the Debye temperature $\theta_D$. Balandin and Wang suggested that a semiconductor quantum well, such as a 10-nm-thick silicon (Si) film, can reduce the phonon group velocity owing to phonon confinement.[11] Thereafter, several studies have confirmed the modification of phonon properties via molecular dynamics (MD).[15,16] However, in many experimental studies on two-dimensional (2D) materials, it was difficult to detect the spatial confinement phenomena. Neogi *et al.*[17] concluded that the thermal conductivities of the sub-30-nm-thick Si films could not be analyzed based on the changes in phonon dispersion; however, the scattering due to the surface roughness ascribed to native oxide adequately described their experimental data. Pettes *et al.*[18] measured the thermal conductivity of 9–25-nm-thick bismuth telluride nanoplates. Diffuse surface scattering resulted in a decrease in the thermal conductivity of sub-20-nm-thick films. This order of reduction is greater than its bulk counterpart.[18] Liu and Asheghi reported that the thermal conductivity of a 20-nm-thick silicon (Si) layer is 22 W/m-K at room temperature, which is lower than the bulk value of 148 W/m-K. This was ascribed to a reduction in the phonon MFP.[19] Wingert *et al.* reported that the thermal conductivity of 15-nm-thick germanium (Ge) nanowires is two times lower than the predicted value; they ascribed this finding to the decrease in phonon MFP and the bulk phonon group velocity.[20] This result suggests that ultra-small nanomaterials could modify the phonon properties by means of the spatial confinement effect. To clarify this context, additional experimental investigations on ultra-thin 2D materials

[a)]J. Kim and H. Kim contributed equally to this work.
[b)]E-mail: woochul@yonsei.ac.kr.

are necessary in order to confirm the modification of phonon properties via spatial confinement.

## II. DETAILS IN EXPERIMENTAL MEASUREMENT

Herein, we demonstrated the effect of phonon confinement, i.e., the modification of phonon dispersion, on the thermal conductivity of nanofilms. High-quality $In_{0.53}Ga_{0.47}As$ single-crystal films were synthesized using the molecular beam epitaxy (MBE) on lattice matched substrates, which minimizes the defects. The thermal conductivities of the 10–70-nm-thick $In_{0.53}Ga_{0.47}As$ nanofilms were measured. To understand how the thermal properties deteriorated, phonon dispersion in $In_{0.53}Ga_{0.47}As$ films of various thicknesses was simulated based on lattice dynamics. The experimental and theoretical results presented in this work are advantageous to elucidate the phonon confinement effect in nanomaterials.

The 10–70-nm-thick $In_{0.53}Ga_{0.47}As$ films were grown on lattice matched InP substrates via molecular beam epitaxy with a base pressure of approximately $10^{-10}$ Torr consistent with the experimental conditions of our previous studies.[21,22] The InP substrate was mounted on molybdenum blocks for uniform substrate heating. The substrate was heated to desorb the native oxide under As overpressure, and $In_{0.52}Al_{0.48}As$ buffer layers were grown to create a smooth and atomically clean surface for $In_{0.53}Ga_{0.47}As$ film growth. The single crystallinity of the as-deposited films was confirmed using small-angle X-ray diffraction (XRD). The small angle XRD was performed on deposited samples by using Ultima model XRD, Rigaku, Japan. By avoiding complex structural analysis, we have performed a simple study to analyze the crystallinity of the deposited films. XRD is widely used for crystal structure and phase identification. Although it is a surface characterization technique, X-rays can penetrate to depths ranging from a few nm to a micron.[23] We have analyzed both sides of the deposited $In_{0.53}Ga_{0.47}As$/InP, as can be seen in Fig. 1, which shows the XRD patterns of 30-nm-thick $In_{0.53}Ga_{0.47}As$/InP [Fig. 1(a)] and 10-nm-thick $In_{0.53}Ga_{0.47}As$/InP [Fig. 1(b)]. The peaks at around 43.8°, 37.56°, and 30.15° resemble those of InP (220), In (110), and $In_{0.53}Ga_{0.47}As$ (200), respectively. The results of this phase analysis agree well with JCPDS 32-0452, JCPDS 03-065-9682, and other literature studies.[24–26] The peak position at 37.56° does not correspond to $In_{0.53}Ga_{0.47}As$, InP, or any oxide; instead, it corresponds to In metal, which could be because of the fact that during the MBE process, excessive In could have been deposited.[27] However, the peak intensity of In/InP reflections decreased gradually when X-rays were incident on the surface of $In_{0.53}Ga_{0.47}As$, which signifies that the In peak position is related to the InAlAs-InP layer. Hereby, no other diffraction peaks of $In_{0.53}Ga_{0.47}As$ were detected, which confirmed that the $In_{0.53}Ga_{0.47}As$ is single-crystalline. The ~2.94 Å and ~5.895 Å d-spacing and lattice constant, respectively, of $In_{0.53}Ga_{0.47}As$ match with the original calculated value, while the InP peak matches with the 220 reflection having a lattice constant of 5.85 Å. In the case of the 10-nm-thick $In_{0.53}Ga_{0.47}As$, owing to the small thickness of the deposited films, X-rays penetrate more across the film depth, and hence, a few traces of InAs are observed between 25°
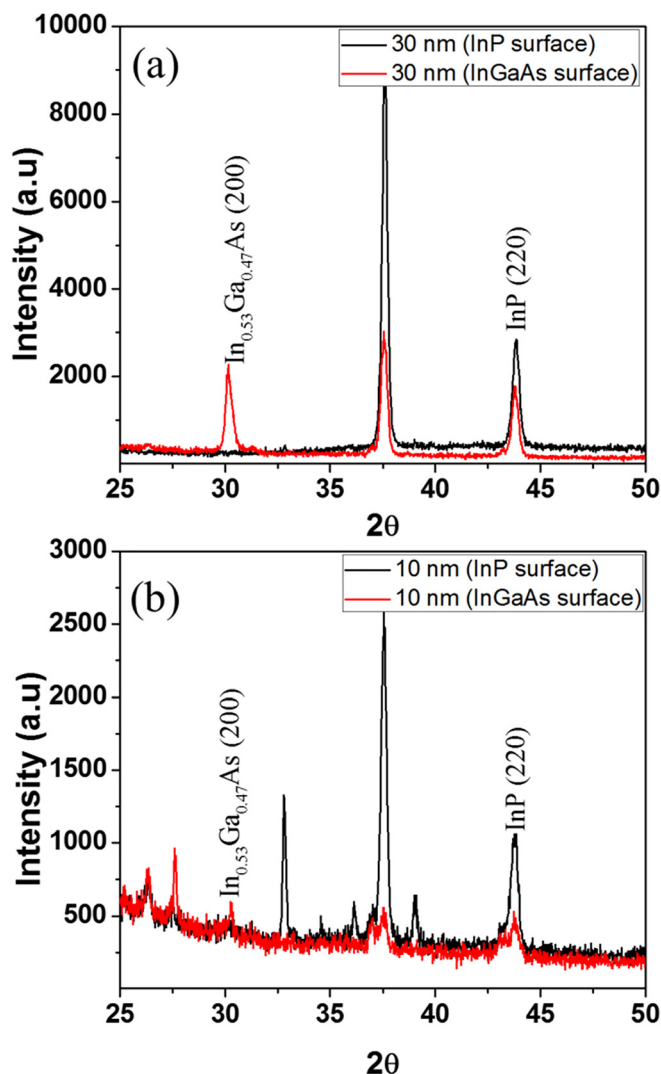


FIG. 1. XRD patterns of (a) 30-nm-thick $In_{0.53}Ga_{0.47}As$/InP and (b) 10-nm-thick $In_{0.53}Ga_{0.47}As$/InP [recorded from InP (black line) and grown $In_{0.53}Ga_{0.47}As$ (red line) surfaces].

and 27°. Given that the $In_{0.53}Ga_{0.47}As$ deposition is performed on $In_{0.52}Al_{0.48}As$, those traces are quantified with the buffer layer.

For measuring the thermal conductivity, first, the substrate was removed to make the $In_{0.53}Ga_{0.47}As$ nanofilms. To do this, we attached the $In_{0.53}Ga_{0.47}As$ films on slide glasses by using crystal bonds, which made it easy for handling the materials. Hydrochloric acid (HCl) was used to selectively etch the InP substrate, and the $In_{0.52}Al_{0.48}As$ buffer layer while leaving the $In_{0.53}Ga_{0.47}As$ films intact. Furthermore, the $In_{0.53}Ga_{0.47}As$ films were soaked in acetone for removing the crystal bond. The nanofilms were transferred to a device for thermal conductivity measurement using a drop-dry technique.[18,28–30] The measurement device was then rinsed in acetone to clean any bonding residue. Figure 2 shows the SEM images of the 10-, 20-, 30-, and 70-nm-thick $In_{0.53}Ga_{0.47}As$ nanofilms on the measurement device.

To investigate whether the chemically etched $In_{0.53}Ga_{0.47}As$ nanofilm (10 nm) retained its single crystallinity, transmission electron microscopy (TEM) was performed. The inset of Fig. 2(a) presents a fast Fourier transform (FFT)
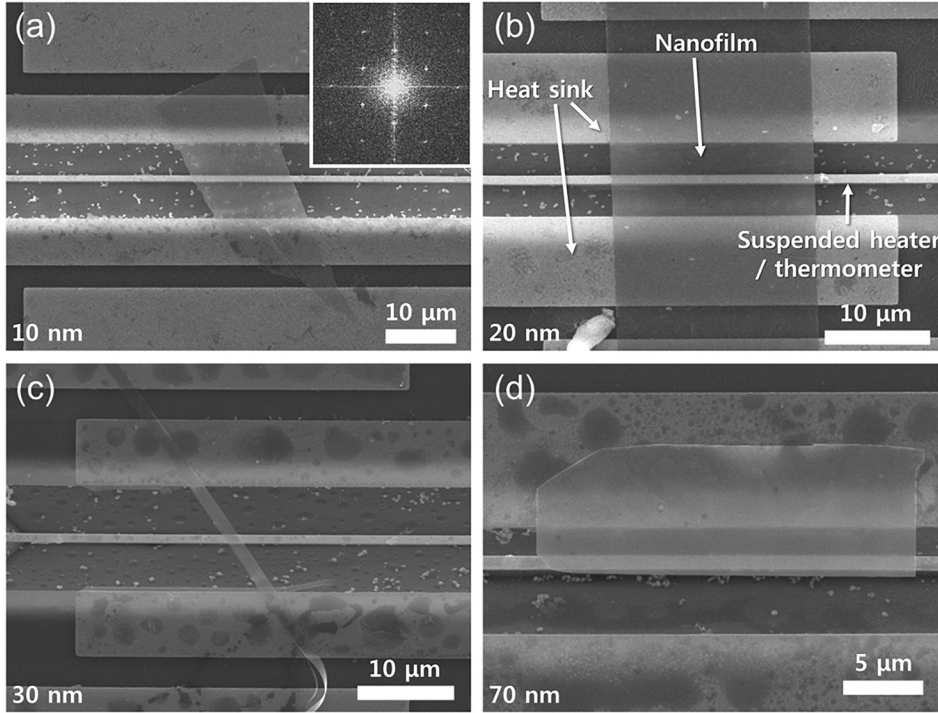
FIG. 2. SEM images of (a) 10-, (b) 20-, (c) 30-, and (d) 70-nm-thick In$_{0.53}$Ga$_{0.47}$As nanofilms. The inset in (a) shows a transmission electron microscopy (TEM) fast Fourier transform (FFT) image of a 10-nm-thick film, suggesting In$_{0.53}$Ga$_{0.47}$As with the single-crystalline order.

image of free-standing In$_{0.53}$Ga$_{0.47}$As showing a single-crystalline order. The XRD patterns exhibit good agreement with the single phase and the crystalline order of In$_{0.53}$Ga$_{0.47}$As. Thus, we confirmed that the nanofilms retain their single crystallinity even after the removal of the substrates.

The thermal conductivities of the nanofilms were measured using the modified T-bridge method. The T-bridge method was originally developed to measure the thermal conductivity of one-dimensional (1D) nanowires and/or nanotubes.[31,32] Later, we modified and updated the technique to measure the thermal conductivity of 2D materials.[33] Although the details of this measurement method are available in our previous publication,[33] a brief explanation is provided herein. By passing a current through a suspended heater, Joule heating is generated [Fig. 2(b)]. The suspended heater also functions as a thermometer, so any rise in its temperature is recorded. The generated heat can only be dissipated through either a 2D material or the suspended heater to the heat sink. The temperature increase in the suspended heater depends on the thermal resistance of the 2D material. For example, if the thermal resistance of the 2D material is small, Joule heat is preferentially transported through the 2D material. Then, the temperature rise of the suspended heater will be insignificant. Therefore, by measuring the temperature rise of the suspended heater, the thermal conductivity of the nanofilms can be determined.

## III. RESULTS AND DISCUSSION

Figure 3(a) shows the experimental results of the thermal conductivity 10-, 20-, 30-, and 70-nm- thick and bulk[34] (1.4 $\mu$m thick) In$_{0.53}$Ga$_{0.47}$As as represented by dots. The Callaway model[35] under the relaxation time approximation with Debye dispersion was used to explain the experimental

data. It is well known that alloy atoms scatter high frequency phonons[36] so that their contribution to thermal transport can be negligible. With this reason, a cutoff frequency and a linear dispersion relationship were used to calculate thermal conductivity of the SiGe alloy.[37,38] This justifies our use of the Debye model. In$_{0.53}$Ga$_{0.47}$As is a semiconducting material with no intentional doping; hence, the contribution of electrons to thermal conductivity is assumed to be small and neglected in theoretical calculations. To calculate the lattice thermal conductivity, $k$, the Callaway model[35] was used, which is based on the Boltzmann transport equation with the relaxation time approximation shown in Eqs. (1)–(4). The Callaway's model[35] with the Debye dispersion, which ignores polarization, was used. Thermal conductivity is expressed as follows:

$$k = \frac{k_B}{2\pi^2 v_g} \left( \frac{k_B T}{\hbar} \right)^3 \left( I_1 + \frac{I_2^2}{I_3} \right), \tag{1}$$

where

$$I_1 = \int_0^{\frac{\theta_D}{T}} \tau_c \frac{x^4 e^x}{(e^x - 1)^2} dx, \tag{2}$$

$$I_2 = \int_0^{\frac{\theta_D}{T}} \frac{\tau_c}{\tau_N} \frac{x^4 e^x}{(e^x - 1)^2} dx, \tag{3}$$

and

$$I_3 = \int_0^{\frac{\theta_D}{T}} \frac{1}{\tau_N} \left( 1 - \frac{\tau_c}{\tau_N} \right) \frac{x^4 e^x}{(e^x - 1)^2} dx, \tag{4}$$

where $v_g$ is the phonon group velocity (speed of sound), $\theta_D$ is the Debye temperature, $x$ is the normalized frequency, $\hbar \omega / k_B T$, and $T$ is the absolute temperature. The combined
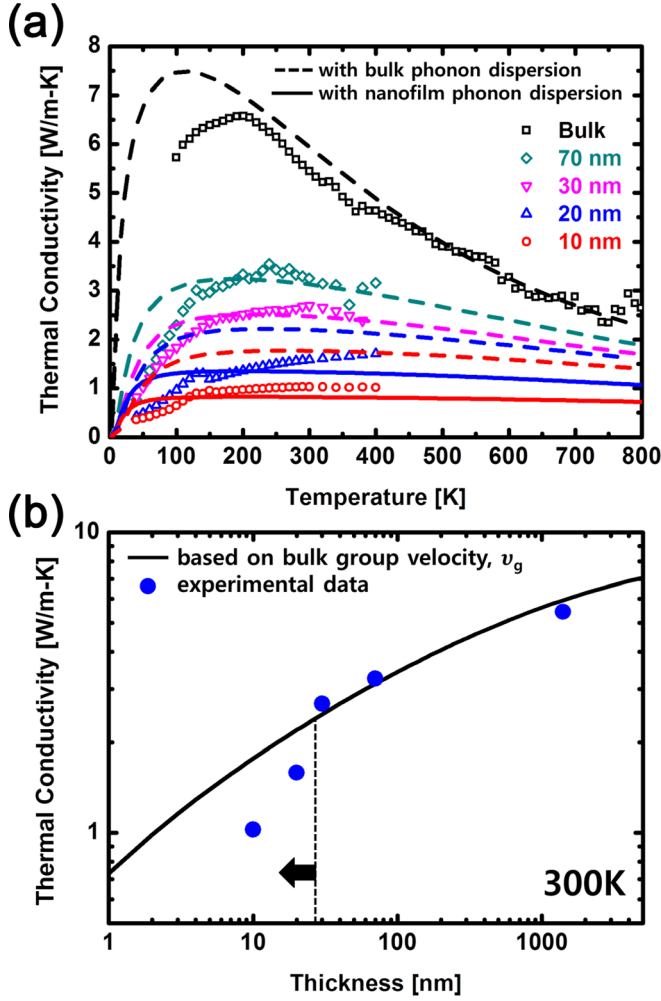
**(a)**



**(b)**



FIG. 3. (a) Temperature-dependent thermal conductivity of In$_{0.53}$Ga$_{0.47}$As. Dots are based on experimental data, whereas dashed and solid lines are drawn by theoretical analysis based on the bulk and nanofilm phonon dispersions, respectively. As shown in the figure, the thermal conductivity calculation based on phonon confinement adequately explains the experimental data of the 20-nm- and 10-nm-thick nanofilms. (b) The thermal conductivities of In$_{0.53}$Ga$_{0.47}$As at 300 K versus thickness. The solid line is based on simulation with bulk group velocity, $v_g$, and dots are based on experimental data. It shows clearly that thermal conductivities of 10 nm and 20 nm thick In$_{0.53}$Ga$_{0.47}$As nanofilms cannot be explained by the theory based on the bulk group velocity.

relaxation time for the bulk determined using Matthiessen's rule[39] explains the dependency on scattering through other factors, as can be seen in the following equation:

$$\tau_{bulk}^{-1} = \tau_U^{-1} + \tau_N^{-1} + \tau_A^{-1}, \tag{5}$$

where $\tau_U$, $\tau_N$, and $\tau_A$ are the relaxation times of Umklapp scattering, normal scattering, and defect or alloy scattering, respectively. The following are respective expressions of the relaxation times in Eq. (5), where $\omega$, $T$, and $l$ are phonon frequency, absolute temperature, and thickness of the thin film, respectively:

$$\tau_U^{-1} = B_U \omega^2 T e^{\frac{-\theta_D}{nT}}, \tag{6}$$

$$\tau_N^{-1} = B_N \omega^2 T^3, \tag{7}$$

$$\tau_A^{-1} = A \omega^4. \tag{8}$$

The relaxation time expressions from Slack *et al.*[40] are given by Eqs. (6) and (7). Table I lists the constants used in Eqs. (6)–(8); these fit the experimental data of thermal conductivity of 1.4-$\mu$m-thick[34] In$_{0.53}$Ga$_{0.47}$As, in Fig. 4(a). The combined relaxation time is calculated by the model suggested by Tang *et al.*[41] which considers the boundary scattering effect on the mean free path of phonons in 2D thin films. The combined mean free path is able to be evaluated by the thickness of the thin film, $d$, and the bulk mean free path, $\ell_{bulk}$, where $\ell_{bulk}, = v_g \tau_{bulk}$. The combined mean free path of phonon is expressed in Eq. (9) with the corresponding combined relaxation time in Eq. (10)

$$\ell_1 = \frac{\ell_{bulk}^2}{d} \int_0^{d/\ell_{bulk}} \left[ 1 + (\gamma - 1)e^{-\gamma} - \gamma^2 \int_\lambda^\infty \frac{e^{-t}}{t} dt \right] d\gamma,$$

$$\ell_2 = \ell_{bulk} \left[ 1 - e^{-d/\ell_{bulk}} + \frac{d}{\ell_{bulk}} e^{-d/\ell_{bulk}} - \left( \frac{d}{\ell_{bulk}} \right)^2 \int_{d/\ell_{bulk}}^\infty \frac{e^{-t}}{t} dt \right],$$

$$\ell_c = \frac{\ell_1 + \ell_2}{2}. \tag{9}$$

The combined mean free path can be calculated as an average value of mean free paths from two parts. Bulk scattering mechanisms denote phonon-phonon scattering and the alloy scattering. Another part is due to the boundary scattering from the thin film. The combined mean free path is the average value of these two separate mean free paths

$$\tau_c = \frac{\ell_c}{v_g}. \tag{10}$$

Table I lists the constants used in the analysis to fit experimental data of thermal conductivity 1.4-$\mu$m-thick In$_{0.53}$Ga$_{0.47}$As. Although thermal conductivity prediction based on the full phonon dispersion would provide precise match on experimental data, the over- or underestimation due to the use of the Debye approximation could be ruled out in comparison of deviations in thermal conductivities of nanofilms as long as the same model is applied to all the materials used in this study.

For calculating the phonon dispersion relationship, the interatomic potential is required, and for In$_{0.53}$Ga$_{0.47}$As, the Tersoff potential has been used so far.[42–50] The Tersoff potential parameters put forth by Ashu *et al.*[50] and Adhikari and Kumar[49] were further used in this calculation, as given in Table II. For forming a supercell, it is convenient to extend the primitive cell to an eight-atom conventional cell having the simple cubic (SC) structure along orthogonal axes. The structures of these films of various thicknesses were established by stacking $N$ conventional unit cells along the out-of-plane direction with thickness $t$, as shown in Fig. 5. The phonon dispersion of the In$_{0.53}$Ga$_{0.47}$As films was calculated using the general utility lattice program

TABLE I. Constants in used in the Callaway model [Eqs. (6)–(8)].

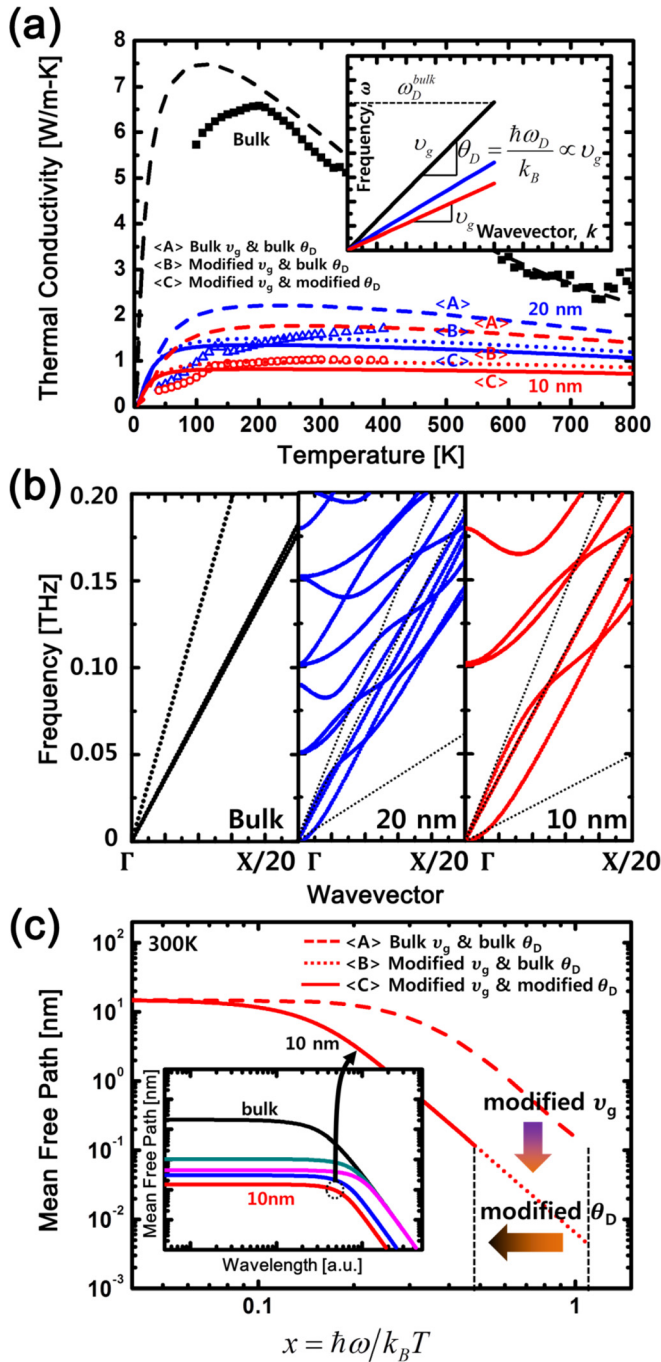| $B_N$ (s/K) | $B_U$ (s/K$^3$) | n | A |
| --- | --- | --- | --- |
| $2.91 \times 10^{-24}$ | $6.46 \times 10^{-19}$ | 1.2 | $8.22 \times 10^{-42}$ |

FIG. 4. (a) Thermal conductivities of the bulk, the 10 nm and 20 nm thick In$_{0.53}$Ga$_{0.47}$As with theoretical calculation based on ⟨A⟩ bulk $v_g$, and bulk Debye temperature, $\theta_D$, ⟨B⟩ modified $v_g$, and bulk $\theta_D$, and ⟨C⟩ modified $v_g$, and modified $\theta_D$. The results obtained using the Callaway model based on the bulk $v_g$ and the $\theta_D$ deviate from the experimental data. In contrast, the results of the Callaway model based on the modified $v_g$ and the $\theta_D$ owing to phonon confinement are closer to the experimental data. Inset shows phonon dispersion based on the Debye approximation, where $v_g$ and $\theta_D$ of the bulk, the 10 nm and 20 nm thick In$_{0.53}$Ga$_{0.47}$As are presented, extracted based on (b) calculated phonon dispersions of the bulk, the 10 nm and 20 nm thick In$_{0.53}$Ga$_{0.47}$As. (c) Phonon mean free path of 10 nm thick In$_{0.53}$Ga$_{0.47}$As nanofilm at 300 K versus phonon frequency, $x$, showing effects of modified $v_g$ and the $\theta_D$ on the phonon mean free path. The inset also shows phonon mean free paths of In$_{0.53}$Ga$_{0.47}$As.

TABLE II. Parameter of Tersoff potential from Sayed *et al.*,[46] except In-Ga, which is from Adhikari and Kumar *et al.*[49]

|  | As-As | In-Ga | In-In | In-As | Ga-Ga | Ga-As |
|---|---|---|---|---|---|---|
| $A_{ij}$ (eV) | 1571.86 | 1214.917 | 2975.54 | 1968.295443 | 993.88 | 2579.46 |
| $B_{ij}$ (eV) | 546.431 | 177.22 | 360.61 | 266.571631 | 136.123 | 317.21 |
| $\lambda_{ij}$ (Å$^{-1}$) | 2.38413 | 2.5621 | 2.6159 | 2.597556 | 2.50842 | 2.82805 |
| $\mu_{ij}$ (Å$^{-1}$) | 1.72872 | 1.58600 | 1.68117 | 1.422429 | 1.49082 | 1.72303 |
| $R_{ij}$ (Å) | 3.4 | 3.4 | 3.4 | 3.5 | 3.4 | 3.4 |
| $S_{ij}$ (Å) | 3.6 | 3.6 | 3.6 | 3.7 | 3.6 | 3.6 |
| $\beta_{ij}$ | 0.007488 | 0.70524 | 2.10871 | 0.3186402 | 0.23586 | 0.35719 |
| $n_{ij}$ | 0.60879 | 3.43739 | 3.40223 | 0.7561694 | 3.47290 | 6.31747 |
| $c_i$ | 5.27313 | 0.080256 | 0.084215 | 5.172421 | 0.076297 | 1.22630 |
| $d_i$ | 0.75102 | 195.2950 | 19.2626 | 1.665967 | 19.7964 | 0.79040 |
| $h_i$ | 0.15292 | 7.26910 | 7.39228 | −0.5413316 | 7.14591 | −0.51848 |

*et al.*[50] and Adhikari and Kumar[49] were further used in this calculation, as given in Table II.

When modeling a phonon wave of the scale of tens of nanometers, the material needs to be considered a discrete structure without periodicity. Crystalline InAs or GaAs contains a two-atom primitive basis, which is extended along a face-centered cubic (FCC) structure. Figure 5(a) shows the two-atom primitive basis. The lattice vectors are non-orthogonal, with a 60° angle between the lattice vectors and the primitive basis. The ΓX direction is the propagation direction in this measurement, as shown in Fig. 5. For forming a supercell, it is convenient to extend the primitive cell to an eight-atom conventional cell having the simple cubic (SC) structure along orthogonal axes. The structures of these films of various thicknesses were established by stacking $N$ conventional unit cells along the out-of-plane direction with thickness $t$, as shown in Fig. 5(c). The in-plane structure has the periodicity required to form a 2D material along the $x$ and $y$ directions. Therefore, the Brillouin zone is modified by a break of periodicity along the out-of-plane direction.

The phonon dispersion of the In$_{0.53}$Ga$_{0.47}$As films was calculated using GULP.[51,52] For reducing the calculation time, In$_{0.47}$Ga$_{0.53}$As is simplified to In$_{0.5}$Ga$_{0.5}$As with a conventional unit cell lattice constant of ~5.5885 Å, which matches with experimental results because these two structures have rather similar phonon dispersions and phonon speeds of sound.[53] The phonon dispersion relationship of bulk In$_{0.5}$Ga$_{0.5}$As is shown in Fig. 6(a). The phonon group velocity of In$_{0.5}$Ga$_{0.5}$As is 3053.3 m/s, which is different from the experimental value of 3491.9 m/s and is based on the average values of In$_{0.53}$Ga$_{0.47}$As for three different acoustic modes.[54]

We obtained the phonon dispersion relationship for bulk In$_{0.5}$Ga$_{0.5}$As and In$_{0.5}$Ga$_{0.5}$As nanofilms of various thicknesses, as shown in Figs. 6(b)–6(e). Considering the structure and lattice dynamics, the phonon group velocities of each branch are 2827.3 m/s for TA and 3652.6 m/s for LA in bulk materials. Furthermore, for calculation of phonon dispersion, there are many branches (especially due to the thin film) due to the number of atoms in the unit cell. To apply Debye approximation for phonon group velocity, we obtained the group velocity of three acoustic modes near the Γ point. The dashed line in Fig. 7 represents the group velocity of the

(GULP).[51,52] For calculating the phonon dispersion relationship, the interatomic potential is required, and for In$_{0.53}$Ga$_{0.47}$As, the Tersoff potential has been used so far.[42–50] The Tersoff potential parameters put forth by Ashu
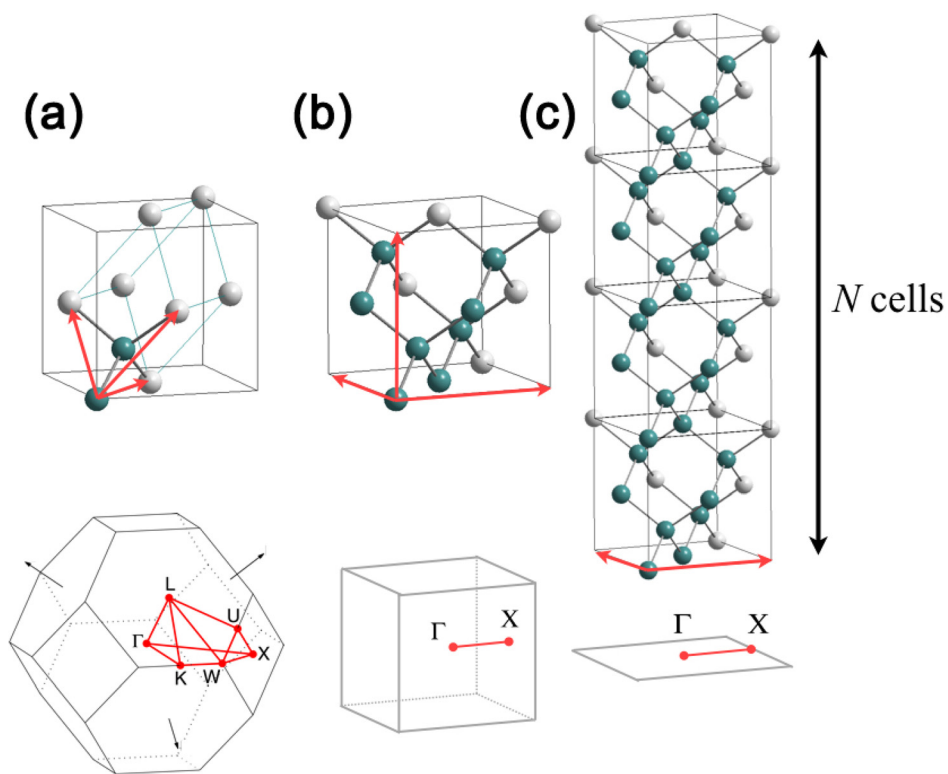
FIG. 5. Crystalline structure and Brillouin Zone with (a) primitive unit cell, (b) conventional unit cell, and (c) thin film unit cell with *N*-layered conventional cells.
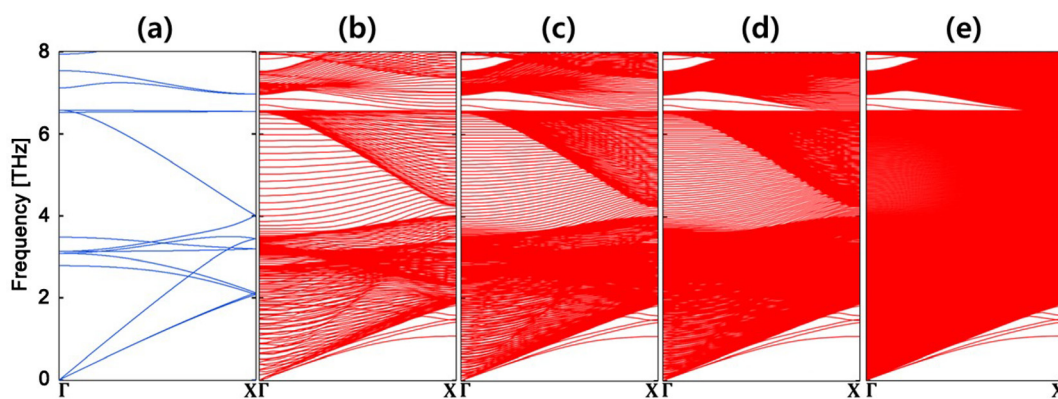


FIG. 6. Phonon dispersion of In$_{0.5}$Ga$_{0.5}$As in (a) bulk and (b) 10 nm, (c) 20 nm, (d) 30 nm, and (e) 70 nm thickness.
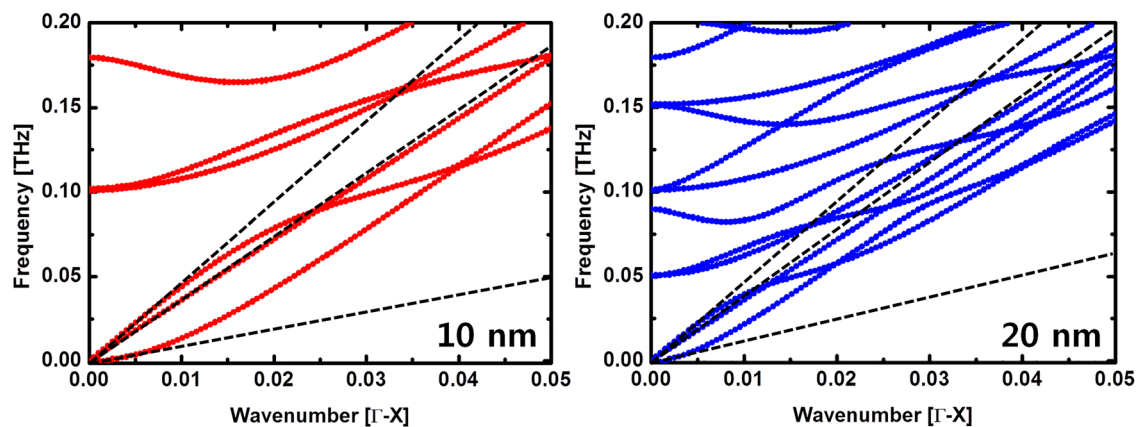


FIG. 7. Phonon dispersion of In$_{0.5}$Ga$_{0.5}$As (a) 10 nm and (b) 20 nm thickness. Each of the dashed lines in phonon dispersion represents the group velocity of two transverse acoustic (TA) and longitudinal acoustic branches (LA), respectively.

three acoustic branches, which is assumed as the speed of sound through thicknesses of 10 and 20 nm; here, K = 0.005, 0, 0 (where the normalized Brillouin Zone boundary is defined by $K_{max} = 0.5, 0, 0$). We noticed that the speed of sound in the 10- and 20-nm-thick decreases as the thickness decreases, and the corresponding value for the 30- and 70-nm-thick films is similar or converge to the bulk value, as given in Table III.

Figure 8 shows phonon mean free paths from Umklapp, alloy, and boundary scatterings and combined mean free paths of the 10-nm-thick $In_{0.5}Ga_{0.5}As$ nanofilm at 300 and 800 K. The solid line corresponds to the case where the phonon in the nanofilm is confined by the nanosize. In this calculation, the modified (reduced) phonon group velocity was chosen followed by the modified Debye temperature. The segmented line is mean free paths when the nanofilm phonon group velocity was assumed to be the bulk group velocity, and the same in the Debye temperature. As in this figure, the combined mean free path with the modified properties (solid) is shorter than the one with the bulk properties (segmented) due to its reduced group velocity and has a short frequency regime due to its reduced Debye temperature. These contribute to the reduced thermal conductivities in $In_{0.5}Ga_{0.5}As$ nanofilms. The results of theoretical analysis of the bulk and nanofilm phonon dispersions are indicated by dashed and solid lines, respectively, in Fig. 3(a). Once the thermal conductivity of the 1.4-$\mu$m-thick $In_{0.53}Ga_{0.47}As$ film was analyzed, the same code, except for the thickness in boundary scattering, was used to fit the experimental data of the $In_{0.53}Ga_{0.47}As$ nanofilms. As shown in Fig. 3(a), the theoretical results of the 30- and 70-nm-thick $In_{0.53}Ga_{0.47}As$ films adequately explain the experimental data, while the deviation between the experimental data and the analytical results is noticeable in the case of the 10- and 20-nm-thick $In_{0.53}Ga_{0.47}As$ films. To further clarify this deviation, the thermal conductivities of $In_{0.53}Ga_{0.47}As$ at 300 K versus thickness are presented in Fig. 3(b). The solid line is based on simulation with bulk group velocity, $v_g$, and dots are based on experimental data. This result suggests that boundary scattering alone cannot describe the thermal conductivity of the 10- and 20-nm-thick $In_{0.53}Ga_{0.47}As$ films. For a more accurate theoretical picture, we have included a phonon confinement effect in the analysis, i.e., modified phonon dispersion, in the analysis.

We noticed that the phonon group velocities, i.e., the speed of sound, are reduced in the case of the 10- and 20-nm-thick nanofilms as in Fig. 7, while those in the case of the 30- and 70-nm-thick nanofilms are appeared to be similar

TABLE III. Speed of sound when K = 0.005, 0, 0 for various film thicknesses. TA and LA stand for transverse acoustic and longitudinal acoustic branches, respectively.

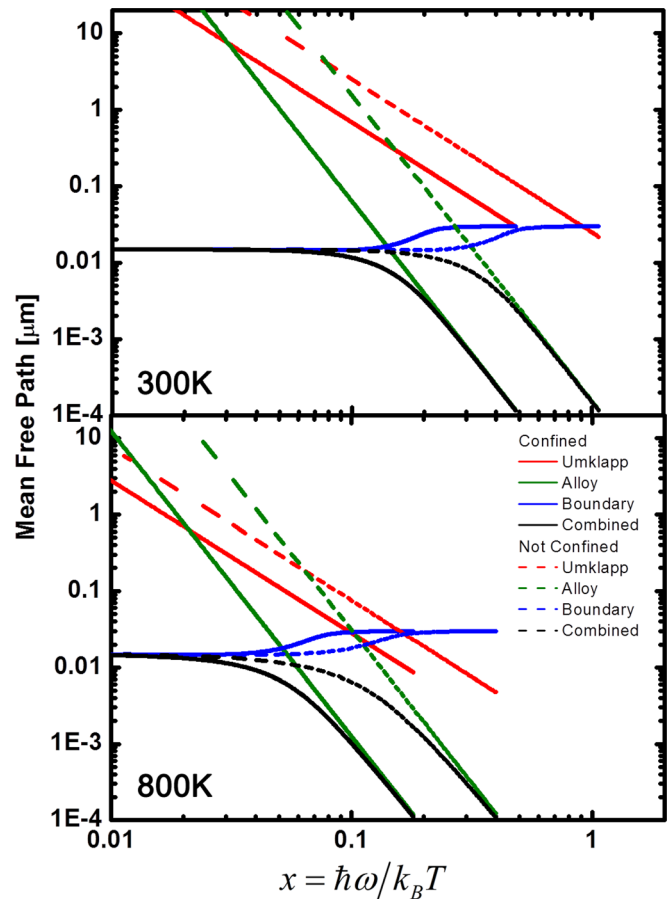| Speed of sound (m/s) | 10 nm | 20 nm | Bulk |
|---|---|---|---|
| TA | 978.5 | 1346.3 | 2827.3 |
| TA | 2540.7 | 2558.1 | 2827.3 |
| LA | 3048.0 | 2999.5 | 3652.6 |
| Debye (average) | 1371.2 | 1809.2 | 3053.3 |



FIG. 8. Phonon mean free paths according to Umklapp, alloy, and boundary scatterings and combined phonon mean free paths of 10 nm $In_{0.5}Ga_{0.5}As$ thin films at 300 K and 800 K. The solid line corresponds to the phonon-confined case with reduced group velocity of the thin film and the dotted line corresponds to the one with bulk group velocity.

to the bulk value, which is 3053.3 m/s. The changes in phonon dispersion affect the phonon group velocity $v_g$, the Debye temperature $\theta_D$, and the phonon DOS. The phonon DOS modifies the phonon heat capacity; however, changes in phonon heat capacity could occur in considerably thin nanofilms (<5 nm) at low temperatures (<20 K).[2] Therefore, we excluded the possibility of changes in the phonon DOS. The modified phonon group velocity affects the Debye cutoff frequency $\omega_D = v_g \times k_D$, which leads to changes in the Debye temperature $\theta_D = h\omega_D/(2\pi k_B)$.

Figure 4(a) shows the thermal conductivities of the bulk, 10 nm, and 20 nm thick $In_{0.53}Ga_{0.47}As$. Here, the theoretical thermal conductivities marked as $\langle A \rangle$, $\langle B \rangle$, $\langle C \rangle$ correspond to different calculation conditions. The line a used the bulk group velocity, $v_g$, and the bulk Debye temperature, $\theta_D$, in the thermal conductivity calculation of the thin film. These lines expect higher thermal conductivities than experimental ones in both thin films below 20 nm thickness. However, sub-20-nm thin films have lower group velocities than the bulk as shown in the inset of Fig. 4(a), which is the modified phonon dispersion based on Debye approximation. The phonon group velocity of the 10-nm-thick nanofilm is half that of the bulk sample. The changes in phonon dispersion affect not only the phonon group velocity but also the Debye temperature. The reduced phonon group velocity decreases the

transport velocity of phonons, thereby leading to a decrease in the thermal conductivity. The low Debye temperature indicates that the range of the phonon spectrum shrinks, which also leads to reduced thermal conductivity. As shown in Fig. 4(a), by adding these effects one by one, namely, the phonon group velocity and the Debye temperature, the thermal conductivity decreases.

Figure 4(c), which shows phonon mean free path of 10 nm $In_{0.53}Ga_{0.47}As$ nanofilm versus phonon frequency, explains why these calculation conditions gives gradually reduced thermal conductivities. From the combined mean free paths of $In_{0.53}Ga_{0.47}As$ films at 300 K shown in the inset of Fig. 4(c), the mean free path of the 10 nm $In_{0.53}Ga_{0.47}As$ nanofilm is chosen as a representative example and presented to explain effects of modified $v_g$ and the $\theta_D$ on the phonon mean free path. With the bulk group velocity and the bulk Debye temperature, the combined mean free path $\langle A \rangle$ is evaluated as long and having a short wavelength regime. Due to the modified group velocity which is slower than one of the bulk, the mean free path becomes shorter $\langle B \rangle$ than $\langle A \rangle$. Here, we should consider the modified Debye temperature since the group velocity is reduced as in the thin film. This makes the regime of the phonon frequency to be short followed by the reduced integral domain in the Debye-Callaway model, as represented in the line $\langle C \rangle$ in Fig. 4(c). This theoretical thermal conductivity as the line $\langle C \rangle$ adequately explains sub-20-nm thin film thermal conductivity well.

The results show that phonon dispersion in considerably thin or small-diameter nanomaterials could be modified, and such modification leads to decreased thermal conductivity. In fact, there are experimental reports focusing on the changes in the phonon group velocity.[55,56] Kwon *et al.*[2] showed that silicon and germanium nanostructures have certain critical values of thickness where the phonon transport phenomena drastically change into the confinement regime. Cuffe *et al.*[55] observed phonon dispersion modification in sub-30-nm-thick Si nanofilms. Jurgilaitis *et al.*[56] measured phonon dispersion in 50-nm-thick InSb nanowires using time-resolved XRD and found that the speed of sound is only 74% of that in the bulk counterpart. They also found that the elastic constant was reduced by 35% compared to the bulk value. This reduced elastic constant is expected based on the relationship of the speed of sound, i.e., the phonon group velocity $v_g = (E/\rho)^{0.5}$, where $E$ and $\rho$ are Young's modulus and density, respectively. Based on the XRD data shown in Fig. 1 and the lattice constant of bulk $In_{0.53}Ga_{0.47}As$,[57] the lattice constant of the $In_{0.53}Ga_{0.47}As$ film is 5.868 Å, whereas those of the 20- and 10-nm-thick $In_{0.53}Ga_{0.47}As$ films are 5.922 and 5.895 Å, respectively. The variation in the lattice constant is less than 1%; thus, reduced Young's modulus is the main reason for the decreased phonon group velocity. This elastic softening has been reported in sub-30-nm-thick Si nanowires,[58] sub-30-nm-thick Si nanotubes,[59] and Si cantilevers.[60,61] Wingert *et al.*[59] observed a sixfold reduction in Young's modulus compared to bulk Si based on the experimental measurements. In this study, the phonon group velocity of the 10-nm-thick $In_{0.53}Ga_{0.47}As$ film is 55% lower than that of bulk $In_{0.53}Ga_{0.47}As$ as in Table III. In addition, we observed an around 3.3-fold reduction in Young's modulus in the case of the 10-nm-thick $In_{0.53}Ga_{0.47}As$ nanofilm. The dependence of the Debye temperature on the elastic constant is known.[62] The changes in the elastic constants are followed by modification in the Debye temperature.

Figure 8 shows the calculated individual MFPs according to the Umklapp, alloy, and boundary scatterings. Additionally, it shows the effective MFP of the 10-nm-thick $In_{0.53}Ga_{0.47}As$ nanofilm at 300 and 800 K. Both the boundary and alloy scatterings are extrinsic effects; thus, the MFPs are governed by the distance between the boundary and alloy atoms. However, changes in phonon dispersion inevitably lead to changes in the selection rules in the phonon–phonon scattering process. Consequently, Umklapp scattering should be affected. The appearance of the Debye temperature in the Umklapp relaxation time as in Eq. (6) is the reason for this finding. While there could be materials for which this intrinsic scattering process, i.e., the Umklapp and normal scatterings, is important, we can conclude that the changes in the MFP of the $In_{0.53}Ga_{0.47}As$ nanofilms were not observed. This further supports the assertion that the modification of the phonon group velocity and the Debye temperature due to the changes in the phonon dispersion is the main reason for the reduction in the thermal conductivity when phonon confinement occurs.

## IV. SUMMARY

In summary, the thermal conductivities of 10–70-nm-thick $In_{0.53}Ga_{0.47}As$ nanofilms were measured. The experimental results reveal that there was a decrease in the thermal conductivity due to a decrease in the film thickness; however, we found that the reason for this decrease depends on the thickness. The reduction of the thermal conductivities of the 30- and 70-nm-thick $In_{0.53}Ga_{0.47}As$ nanofilms was caused by severe phonon boundary scattering. However, the thermal conductivities of the 10- and 20-nm-thick $In_{0.53}Ga_{0.47}As$ nanofilms were lower than the Casimir limit. Our analysis indicates that phonon confinement occurred in the 10- and 20-nm-thick $In_{0.53}Ga_{0.47}As$ nanofilms; thus, the changes in phonon dispersion were found to modify the phonon group velocity and the Debye temperature. This result suggests that thermal transport in solids can be manipulated not only by phonon boundary scattering but also by phonon confinement effects.

## ACKNOWLEDGMENTS

[1]W. Kim, R. Wang, and A. Majumdar, Nano Today **2**, 40 (2007).
[2]S. Kwon, M. C. Wingert, J. L. Zheng, J. Xiang, and R. K. Chen, Nanoscale **8**, 13155 (2016).
[3]D. Y. Li, Y. Wu, R. Fan, P. D. Yang, and A. Majumdar, Appl. Phys. Lett. **83**, 3186 (2003).
[4]R. Chen, A. I. Hochbaum, P. Murphy, J. Moore, P. D. Yang, and A. Majumdar, Phys. Rev. Lett. **101**, 105501 (2008).

[5]A. I. Boukai, Y. Bunimovich, J. Tahir-Kheli, J. K. Yu, W. A. Goddard, and J. R. Heath, Nature **451**, 168 (2008).

[6]H. Kim, I. Kim, H. J. Choi, and W. Kim, Appl. Phys. Lett. **96**, 233106 (2010).

[7]A. L. Moore, M. T. Pettes, F. Zhou, and L. Shi, J. Appl. Phys. **106**, 034310 (2009).

[8]J. W. Roh, K. Hippalgaonkar, J. H. Ham, R. K. Chen, M. Z. Li, P. Ercius, A. Majumdar, W. Kim, and W. Lee, ACS Nano **5**, 3954 (2011).

[9]J. W. Roh, S. Y. Jang, J. Kang, S. Lee, J. S. Noh, W. Kim, J. Park, and W. Lee, Appl. Phys. Lett. **96**, 103101 (2010).

[10]L. Shi, Nanoscale Microscale Thermophys. Eng. **16**, 79 (2012).

[11]A. Balandin and K. L. Wang, Phys. Rev. B **58**, 1544 (1998).

[12]A. Khitun, A. Balandin, and K. L. Wang, Superlattices Microstruct. **26**, 181 (1999).

[13]J. Zou and A. Balandin, J. Appl. Phys. **89**, 2932 (2001).

[14]G. Chen, *Nanoscale Energy Transport and Conversion: A Parallel Treatment of Electrons, Molecules, Phonons, and Photons (MIT-Pappalardo Series in Mechanical Engineering)* (Oxford University Press, USA, 2005).

[15]J. E. Turney, A. J. H. McGaughey, and C. H. Amon, J. Appl. Phys. **107**, 024317 (2010).

[16]X. J. Wang and B. L. Huang, Sci. Rep. **4**, 6399 (2014).

[17]S. Neogi, J. S. Reparaz, L. F. C. Pereira, B. Graczykowski, M. R. Wagner, M. Sledzinska, A. Shchepetov, M. Prunnila, J. Ahopelto, C. M. Sotomayor-Torres, and D. Donadio, ACS Nano **9**, 3820 (2015).

[18]M. T. Pettes, J. Maassen, I. Jo, M. S. Lundstrom, and L. Shi, Nano Lett. **13**, 5316 (2013).

[19]W. J. Liu and M. Asheghi, Trans. ASME - J. Heat Transfer **128**, 75 (2006).

[20]M. C. Wingert, Z. C. Y. Chen, E. Dechaumphai, J. Moon, J. H. Kim, J. Xiang, and R. K. Chen, Nano Lett. **11**, 5507 (2011).

[21]A. A. Podpirka, J. Shabani, M. B. Katz, M. E. Twigg, S. Mack, C. J. Palmstrom, and B. R. Bennett, J. Appl. Phys. **117**, 245313 (2015).

[22]J. K. Kawasaki, L. I. M. Johansson, B. D. Schultz, and C. J. Palmstrom, Appl. Phys. Lett. **104**, 022109 (2014).

[23]B. D. Cullity, *Elements of X-Ray Diffraction* (Addison-Wesley Publishing Company Inc., Boston, 1978).

[24]F. L. Gao, L. Wen, J. L. Li, Y. F. Guan, S. G. Zhang, and G. Q. Li, CrystEngComm **16**, 10774 (2014).

[25]P. N. Bartlett, D. Cook, C. H. de Groot, A. L. Hector, R. M. Huang, A. Jolleys, G. P. Kissling, W. Levason, S. J. Pearce, and G. Reid, RSC Adv. **3**, 15645 (2013).

[26]S. Carenco, M. Demange, J. Shi, C. Boissiere, C. Sanchez, P. Le Floch, and N. Mezailles, Chem. Commun. **46**, 5578 (2010).

[27]A. Bosacchi, F. Colonna, S. Franchi, P. Pascarella, P. Allegri, and V. Avanzini, J. Cryst. Growth **150**, 185 (1995).

[28]W. Jang, W. Bao, L. Jing, C. N. Lau, and C. Dames, Appl. Phys. Lett. **103**, 133102 (2013).

[29]L. Shi, D. Li, C. Yu, W. Jang, D. Kim, Z. Yao, P. Kim, and A. Majumdar, J. Heat Transfer **125**, 881 (2003).

[30]Y. H. Park, J. Kim, H. J. Choi, H. Kim, I. Kim, K. Y. Lee, D. Seo, and W. Kim, Appl. Phys. A-Mater. Sci. Process. **104**, 7 (2011).

[31]C. Dames, S. Chen, C. T. Harris, J. Y. Huang, Z. F. Ren, M. S. Dresselhaus, and G. Chen, Rev. Sci. Instrum. **78**, 104903 (2007).

[32]M. Fujii, X. Zhang, H. Q. Xie, H. Ago, K. Takahashi, T. Ikuta, H. Abe, and T. Shimizu, Phys. Rev. Lett. **95**, 065502 (2005).

[33]J. Kim, D. J. Seo, D. Park, H. Kim, H. J. Choi, and W. Kim, Rev. Sci. Instrum. **88**, 054902 (2017).

[34]W. Kim, J. Zide, A. Gossard, D. Klenov, S. Stemmer, A. Shakouri, and A. Majumdar, Phys. Rev. Lett. **96**, 045901 (2006).

[35]J. Callaway, Phys. Rev. **113**, 1046 (1959).

[36]B. Abeles, Phys. Rev. **131**, 1906 (1963).

[37]R. Cheaito, J. C. Duda, T. E. Beechem, K. Hattar, J. F. Ihlefeld, D. L. Medlin, M. A. Rodriguez, M. J. Campion, E. S. Piekos, and P. E. Hopkins, Phys. Rev. Lett. **109**, 195901 (2012).

[38]Z. Wang and N. Mingo, Appl. Phys. Lett. **97**, 101903 (2010).

[39]D. M. Rowe, *CRC Handbook of Thermoelectrics* (CRC Press, 1995).

[40]D. T. Morelli, J. P. Heremans, and G. A. Slack, Phys. Rev. B **66**, 195304 (2002).

[41]G. H. Tang, Y. Zhao, G. X. Zhai, and C. Bi, J. Appl. Phys. **110**, 046102 (2011).

[42]J. T. Titantah, D. Lamoen, M. Schowalter, and A. Rosenauer, J. Appl. Phys. **101**, 123508 (2007).

[43]K. Nordlund, J. Peltola, J. Nord, J. Keinonen, and R. S. Averback, J. Appl. Phys. **90**, 1710 (2001).

[44]Y. Nishidate and G. P. Nikishkov, J. Appl. Phys. **102**, 083501 (2007).

[45]K. Albe, K. Nordlund, J. Nord, and A. Kuronen, Phys. Rev. B **66**, 035205 (2002).

[46]M. Sayed, J. H. Jefferson, A. B. Walker, and A. G. Cullis, Nucl. Instrum. Methods Phys. Res., Sect. B **102**, 218 (1995).

[47]D. Powell, M. A. Migliorato, and A. G. Cullis, Phys. Rev. B **75**, 115202 (2007).

[48]J. Adhikari, Comput. Mater. Sci. **43**, 616 (2008).

[49]J. Adhikari and A. Kumar, Mol. Simul. **33**, 623 (2007).

[50]P. A. Ashu, J. H. Jefferson, A. G. Cullis, W. E. Hagston, and C. R. Whitehouse, J. Cryst. Growth **150**, 176 (1995).

[51]E. R. Cope and M. T. Dove, J. Appl. Crystallogr. **40**, 589 (2007).

[52]J. D. Gale and A. L. Rohl, Mol. Simul. **29**, 291 (2003).

[53]M. Salmani-Jelodar, A. Paul, T. Boykin, and G. Klimeck, J. Comput. Electron. **11**, 22 (2012).

[54]S. Adachi, *Physical Properties of III-V Semiconductor Compounds* (John Wiley & Sons, Inc., 1992).

[55]J. Cuffe, E. Chavez, A. Shchepetov, P. O. Chapuis, E. H. El Boudouti, F. Alzina, T. Kehoe, J. Gomis-Bresco, D. Dudek, Y. Pennec, B. Djafari-Rouhani, M. Prunnila, J. Ahopelto, and C. M. S. Torres, Nano Lett. **12**, 3569 (2012).

[56]A. Jurgilaitis, H. Enquist, B. P. Andreasson, A. I. H. Persson, B. M. Borg, P. Caroff, K. A. Dick, M. Harb, H. Linke, R. Nüske, L. E. Wernersson, and J. Larsson, Nano Lett. **14**, 541 (2014).

[57]F. L. Gao, L. Wen, X. N. Zhang, Y. F. Guan, J. L. Li, S. G. Zhang, and G. Q. Li, Thin Solid Films **589**, 32 (2015).

[58]Y. Zhu, F. Xu, Q. Qin, W. Y. Fung, and W. Lu, Nano Lett. **9**, 3934 (2009).

[59]M. C. Wingert, S. Kwon, M. Hu, D. Poulikakos, J. Xiang, and R. K. Chen, Nano Lett. **15**, 2605 (2015).

[60]H. Sadeghian, C. K. Yang, J. F. L. Goosen, A. Bossche, U. Staufer, P. J. French, and F. van Keulen, J. Micromech. Microeng. **20**, 064012 (2010).

[61]H. Sadeghian, C. K. Yang, J. F. L. Goosen, E. van der Drift, A. Bossche, P. J. French, and F. van Keulen, Appl. Phys. Lett. **94**, 221903 (2009).

[62]H. Siethoff and K. Ahlborn, Phys. Status Solidi B **190**, 179 (1995).